PHYSICAL REVIEW B VOLUME 54, NUMBER 8 15 AUGUST 1996-II

Surface-scattering study of the interaction potential of He atoms with the step edges of the Cu(211) and Cu(511) vicinal surfaces

S. Miret-Artes,* J. P. Toennies, and G. Witte
Max-Planck-Institut für Strömungsforschung, Bunsenstraße 10, D-37073 Göttingen, Germany
(Received 22 February 1996)

The diffraction intensities of He atoms scattered from vicinal Cu(211) and Cu(511) surfaces have been measured with a high angular resolution over a wide range of incident energies from 8 to 82 meV. Close-coupling scattering calculations with a corrugated Morse potential were performed to obtain the corrugation parameters for the first three complex Fourier coefficients. The energy-dependent corrugation profiles determined from the best fit indicate that the corrugation predicted by a simple hard-sphere model is considerably smeared out at the small electron densities far from the surface probed by the He atoms. A comparison with Eikonal calculations demonstrates that hard corrugated wall Eikonal models are not adequate for the structural analysis of stepped surfaces. [S0163-1829(96)00831-4]

I. INTRODUCTION

Structural defects at surfaces have long been of great interest because of their crucial role in many important physical and chemical processes that occur only at the solid-vacuum interface: chemical reactions, catalysis, crystal growth, electronic emission, and surface structural transitions.[1] Periodically stepped (vicinal) surfaces are ideal model systems for isolating one type of defect, a step edge, which becomes accessible to study by diffraction techniques. For example, on metal surfaces, diffraction experiments with either He atoms or electrons [low-energy electron diffraction (LEED)] have been recently used to study the structures of stepped surfaces,[2–5] their roughening,[6–8] faceting,[9,10] and the nucleation of growth at step edges.[1,11,12] Helium-atom scattering (HAS) and LEED are largely complimentary diffraction techniques. Whereas LEED is sensitive to the positions of the surface atoms, HAS is uniquely sensitive to the very low density of electrons $[10^{-3}-10^{-5}\ e/(\text{a.u.})^3]$ protruding far out ($\sim$3–4 Å) from the surface of a metal.[13]

Step atoms on metal surfaces are known to show a significant inward relaxation,[14,15] which has been confirmed in a number of LEED and ion-scattering studies.[16,17] It has also been established that the work function decreases with the number of steps from which dipole moments of 0.2–0.6 D per step atom are derived.[18] Furthermore, for step edges an asymmetry in the mobility of adatoms for diffusion across step edges (''Schwoebel effect'') has been found.[11,19,20] This demonstrates clearly a significant charge transfer away from the steps, which is explained by the Smoluchowski effect[21] and is supported by calculations of Tersoff and Falicov[22] and Nelson and Feibelmann.[23] These predicted significant structural and electronic modifications at step sites[15,22–24] could so far not be confirmed by the available HAS experiments despite the fact that HAS is predicted to be sensitive to electronic modifications at the step edges.[25]

The first careful HAS study of the corrugation of a stepped surface was carried out by Lapujoulade and co-workers[2,26] for the Cu(711) stepped surface. These and related studies for the (110), (311), (511), and (711) surfaces of copper were carefully analyzed using the corrugated Morse potential.[3] The results for all except the (711) surface could be fitted by using only two Fourier components with the second-order components being smaller by more than an order of magnitude. This limited amount of information could be shown to be in reasonable agreement with a simple model in which the electronic density at the surface is estimated from a superposition of the charge distribution of individual surface atoms neglecting relaxation. The repulsive part of the potential is then obtained by simple assuming it to be proportional to the charge density.[27,28] This analysis was later confirmed by Cortona, Dondi, and Tommasini.[29] A subsequent He scattering study of Ni(511) by Kaufman *et al.*[4] came to essentially the same conclusions. Despite the large differences in the reactivity of Ni and Cu and in the electron density at the Fermi level for these metals, Kaufman *et al.* found a very similar shape and amplitude of the surface electron density contours for both metals.

Recently, in the search for more detailed microscopic information on special dynamical features that might result from electronic modifications at step edges, Sibener and co-workers[30,31] and Witte *et al.*[32] have investigated the step-localized phonons on the Ni(997) and the Cu(211) and the Cu(511) surfaces, respectively. In the latter study the step phonon modes could be clearly identified and their dispersion in k space along the two main symmetry directions could be traced out. Detailed comparisons with lattice dynamical calculations, however, were not able to identify any significant modifications in the force field at the step edges.

The present experimental and theoretical study is a renewed attempt at finding and isolating modifications in the electronic structure at the step edges based on a HAS diffraction study of the same Cu(211) and (511) surfaces. In the present work the angular resolution is about $\Delta\Theta = 0.2°$, which is considerable better than $\Delta\Theta = 0.6°$ used in the earlier experiments[3,4] of Gorse *et al.* and Kaufman *et al.*

Moreover, in our previous studies of surface phonons we were able to achieve a very high degree of perfection in the structural uniformity of these copper vicinal surfaces. This we shall see is important for obtaining a large number of sharp diffraction peaks. The determination of the He-surface potential from the diffraction data (the so-called inverse problem) is even for an ideal surface by no means an easy task. In order to account for a realistic interaction potential that has both a soft repulsive part as well as the predicted long-range attractive potential the experimental results have been interpreted using close-coupling (CC) quantum-mechanical calculations.[33–35] As in previous theoretical studies of the vicinal copper surfaces,[3] we have used the corrugated Morse potential (CMP) model.[36]

CC calculations can be considered as being essentially nearly exact. These calculations are often very time consuming because of the large number of diffraction channels (N) necessary to obtain numerical convergence (computing time scales with N^3). The number of channels increases with the corrugation of the surface, the size of the unit cell length, the mass, and the incident energy and decreases with the angle of incidence of the incoming particles. Furthermore, for very asymmetric surface corrugation profiles, the number of Fourier coefficients is greater and they are complex. Thus, in order to reproduce the data, a double set of corrugation parameters (real and imaginary parts) have to be fitted, making the problem nearly intractable. To circumvent these problems we have developed a method in which an analytical solution for the energy-dependent Fourier coefficients of the coupling matrix elements is derived. With this procedure it has been possible to fit the diffraction data over a wide range of incident energies, from $E_i = 8$ up to 82 meV, studied.

Fortunately, for the CC calculations in the case of the stepped surfaces considered here, Cu(211) and Cu(511), it can be assumed to a very good approximation that the corrugation is one dimensional and along the direction perpendicular to the step edges. The ideal atomic structures of the Cu(511) and Cu(211) surfaces are shown in Fig. 1. They consist of (100) and (111) terraces, each containing three atom rows separated by monoatomic steps with (111) and (100) faces, respectively. The angles α formed between the terrace plane and the macroscopic surface (i.e., the nominal Miller indexed surface plane) are 15.8° and 19.5° for the Cu(511) and Cu(211) surfaces, respectively. Thus, while both surfaces have nearly the same step separation d, they have complementary terrace and step face orientations. In the calculations we use a coordinate system with the z axis perpendicular to the macroscopic surface. The y axis is chosen to be along the step edge and the x axis perpendicular to the step edge [Fig. 1(c)].

This paper is organized as follows. In Sec. II we describe the apparatus and sample preparation. The diffraction patterns are presented in Sec. III. Section IV describes the approximations used to facilitate the numerical calculations. The comparison of the best fit calculations with the experiments is discussed in Sec. V. The corrugation profiles determined from the best fit show that for these two Cu vicinal surfaces the corrugation is dominated by a few low-order Fourier components. The reasons for no large anomalies due to enhanced electron spillout at the step edges is discussed in Sec. VI.

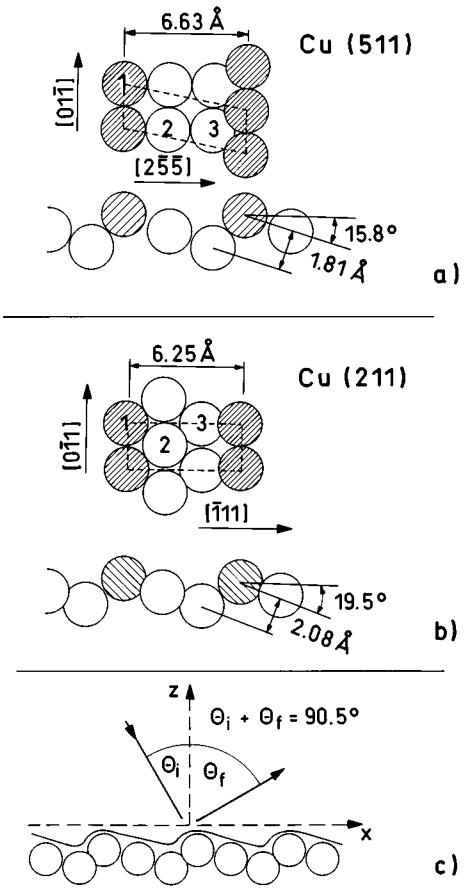

FIG. 1. Geometry of the stepped copper surfaces. The Cu(511) surface (a) consists of (100) terraces with a step separation $d = 6.63$ Å . The Cu(211) surface (b) has (111) oriented terraces and a comparable step distance. (c) illustrates the scattering geometry for the scattering uphill perpendicular to the step edges. The sum of the angle of incidence and of the final scattering direction is constant (90.5°).

II. EXPERIMENTAL SETUP AND SAMPLE PREPARATION

In the He scattering apparatus, which is described in detail elsewhere,[9] a well-collimated nearly monoenergetic helium atom beam is directed at the surface. The scattered atoms are detected at a fixed total scattering angle of 90.5° with respect to the incident beam, while the angle of incidence and the final scattering angle are varied by rotating the crystal. The overall angular resolution of the apparatus is 0.18°. The energy of the He-atom beam can be varied between 8 and 120 meV ($k_i = 4.0$–15.2 Å^{-1}) with an overall velocity distribution of about $\Delta v/v = 0.75\%$ by changing the source temperature from 35 to 500 K, respectively. Because of the fixed total angle geometry the parallel momentum transfer for elastic scattering is given by $\Delta K_{\parallel} = k_i(\sin\theta_i - \sin\theta_f)$, where θ_i is the incident angle and $\theta_f = 90.5° - \theta_i$ [see Fig. 1(c)]: The energy and angular resolution limit the transfer width to about 250 Å .

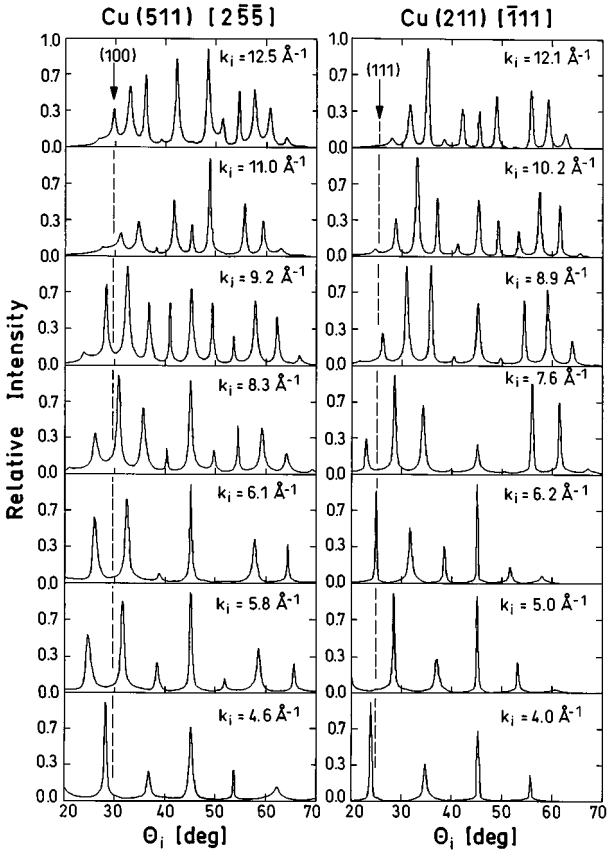

FIG. 2. Series of HAS angular distributions taken (uphill) perpendicular to the step edge direction for the Cu(511) and Cu(211) surfaces. The measurements were performed over a wide range of initial He-atom wave vectors k_i between 4.0 and 12.5 Å^{-1} at crystal temperatures between 100 and 130 K. The dashed vertical lines mark the terrace specular positions.

The copper single crystals with (511) and (211) surfaces, which had been first polished within $\pm 0.1°$ of the desired =orientation, were prepared in UHV (base pressure 1×10^{-10} mba by repeated cycles of Ar^+-ion bombardment (800 eV, 30 min) and subsequent annealing to 800 K. This *in situ* sample preparation procedure was concluded as soon as the helium atom diffraction peaks measured by rotating the crystal show no further narrowing and no traces of sulphur, carbon, and oxygen were found in the recorded x-ray photoemission spectroscopy spectra within the detection limit of 0.5% of a monolayer.

All the HAS measurements were performed at low crystal temperatures of 100–150 K, at which no thermal activated defect formation occurs[11] and the multiphonon excitation is minimized.[37] In a previous investigation[32] the surface phonon dispersion curves were determined over the entire Brillouin zone from a high-resolution time-of-flight analysis of the scattered atoms. This investigation indicated that below 150 K the elastically scattered intensity perpendicular to the steps is about 80% of the total scattering intensity.

III. EXPERIMENTAL RESULTS

Figure 2 shows a series of HAS angular distributions taken over a wide range of initial He-atom wave vectors k_i and incident energies (E_i) between 4.0 (8.4 meV) and 12.5 Å^{-1} (81.6 meV) along the azimuth direction uphill and perpendicular to the step edges. Many intense and sharp diffraction peaks up to the $\pm$ 6th order are observed. From the measured angular positions of the diffraction peaks the average step separations d were determined to be 6.65 (±0.08) Å and 6.28 (±0.08) Å for the Cu(511) and Cu(211) surfaces, respectively. The separation is in agreement within the errors with the ideal separations of 6.62 Å and 6.25 Å . As discussed previously, HAS exhibits very strongly enhanced form factors for step edge atoms in comparison to the diffraction of low energy electrons.[9] Consequently, the observed step edge scattering is relatively intense and this enables a very accurate determination of step separation distributions.[38] For a stepped surface three-dimensional Bragg conditions exist for which the scattering from all steps of the crystal within the coherence length of the incident beam is in phase. For an anti-Bragg (AB) condition the angular full width at half maximum (FWHM) of the diffraction peaks from the macroscopic lattice is determined by the distribution of step separations. After deconvolution with the beam energy width and the angular resolution the surface coherence length perpendicular to the steps is estimated from the FWHM of the step diffraction in the AB condition to be 72 Å and 63 Å corresponding to about ten terraces for the Cu(511) and Cu(211) surfaces, respectively.

For scattering along a direction parallel to the step edges no diffraction peaks within the noise limit of $I/I_{\max}=5\times10^{-5}$ could be observed for the (511) surface. For the Cu(211) surface a weak first-order diffraction peak was observed with an intensity of 3×10^{-3} relative to the specular peak [see Fig. 3(a)]. Since the measured integrated diffraction intensity along the step edges is less then 5×10^{-4} of the integrated diffraction intensity perpendicular to the steps, the surface can be very well approximated by a one-dimensional corrugation function perpendicular to the step edges (x direction). For both surfaces no significant broadening of the width of the specular peak could be observed for angular distributions along the step edge direction. From the peak width an average kink distance of more than 120 Å is estimated. Therefore, we conclude that defects on these surfaces, if at all present, consist mainly of long sections of the step edges that are uniformly shifted perpendicular to the nominal step edges resulting in a distribution of terrace widths.

Figure 3(b) shows the diffraction intensity at the terrace specular condition during a controlled linear variation of the beam source temperature (''drift'' spectrum) that leads to a scan over the incident wave vector.[9] The equidistant intensity maxima as a function of the (elastic) momentum exchange perpendicular to the terraces $\Delta k^{\perp}$ correspond to conditions where atoms are constructively scattered in phase from neighboring terraces. Using the relationship for these maxima, $h=n2\pi/\Delta k^{\perp}$, step heights h of 1.84 (±0.05) Å and 2.03 (±0.05) Å are determined in very good agreement with the expected values of 1.81 Å and 2.08 Å for the ideal Cu(511) and Cu(211) surfaces, respectively. The absence of intermediate maxima and the low diffraction intensity at the out-of-phase conditions (minima) indicate the absence of larger step heights and appreciable faceting. It should be

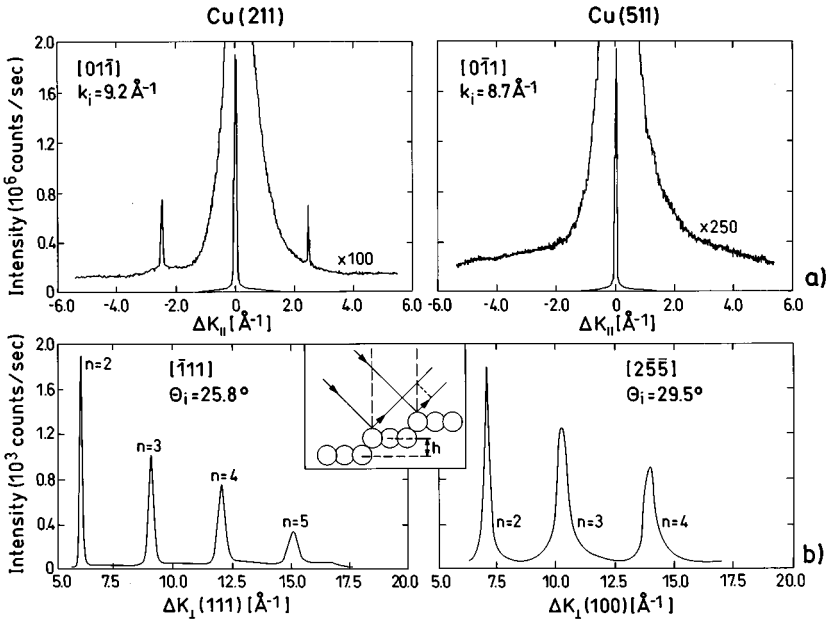

FIG. 3. (a) HAS angular distributions along the step edge direction. (b) Intensity of the (elastic) terrace specular peak (compare Fig. 2) for a controlled variation of the incident He beam energy as a function of the perpendicular momentum transfer. The observed maxima correspond to in-phase conditions for constructive interference between neighboring terraces separated by the step height h (as shown in the inset).

noted, however, that the good agreement of heights with the ideal spacing of bulk planes does not exclude relaxation of step atoms. Since the He-atom form factors are largely determined by the atoms at the step edges, any relaxation with respect to the terraces will be difficult to observe since a relaxation induced shift will be the same for all step edges.

Finally, we mention that angular distributions measured for surface temperatures of 100 and 200 K revealed no significant differences. This result confirms that in this temperature range there is no indication of roughening or faceting, which was also found in a recent energy-resolved He-atom scattering study by Ernst *et al.*[11]

IV. THEORY

A. Model interaction potential

To model the atom-surface interaction potential we have adopted the corrugated Morse potential, originally proposed by Armand and Manson,[36]

$$V(\mathbf{R},z)=D\left[\frac{1}{\mathcal{V}_0}e^{-2\chi[z-\xi(\mathbf{R})]}-2e^{-\chi z}\right], \tag{1}$$

where D is the well depth, χ the stiffness parameter, $\xi(\mathbf{R})$ the corrugation or shape function, and $\mathcal{V}_0$ the surface average of the exponential of the corrugation function. Since $\xi(\mathbf{R})$ is assumed to be periodic, and therefore the term $\exp[2\chi\xi(\mathbf{R})]$, the complete interaction potential $V(\mathbf{R},z)$ is also periodic. Equation (1) is conveniently expanded in a Fourier series

$$V(\mathbf{R},z)=V_0(z)+\sum_{\mathbf{G}\neq\mathbf{0}}V_{\mathbf{G}}(z)e^{i\mathbf{G}\cdot\mathbf{R}}. \tag{2}$$

The potential Fourier coefficients $V_{\mathbf{G}}(z)$ can then be expressed by analytical functions in terms of the corrugation Fourier coefficients $\mathcal{V}_{\mathbf{G}}$ of the periodic exponential term of Eq. (1), which are given by

$$\mathcal{V}_{\mathbf{G}}=\frac{1}{S}\int_{\mathrm{U}}d\mathbf{R}e^{-i\mathbf{G}\cdot\mathbf{R}}e^{2\chi\xi(\mathbf{R})}, \tag{3}$$

where the integration is performed over the unit cell (U) of area S and $\mathbf{G}$ is a reciprocal lattice vector. From Eq. (2), the first Fourier coefficient is given by

$$V_0(z)=D[e^{-2\chi z}-2e^{-\chi z}]. \tag{4}$$

The higher-order terms in the diffraction process are all simply related to the Fourier components of the periodic exponential term by

$$V_{\mathbf{G}}(z)=\frac{D\mathcal{V}_{\mathbf{G}}}{\mathcal{V}_0}e^{-2\chi z}\quad\text{for}\quad\mathbf{G}\neq\mathbf{0}. \tag{5}$$

Without loss of generality, we can expand the corrugation function of the stepped surfaces as

$$\xi(x)\cong\sum_{j=1}^{j_{\max}}|h_j|\cos\left(\alpha_j+\frac{j2\pi}{d}x\right), \tag{6}$$

where d is the step separation (equal to the unit cell length in this direction). This real function can describe asymmetric profiles for stepped surfaces when $\alpha_j\neq 0$. Thus the corresponding corrugation amplitudes can conveniently be expressed in terms of complex parameters given by their real and imaginary parts $\mathrm{Re}(h_j)=|h_j|\cos\alpha_j$ and $\mathrm{Im}(h_j)=|h_j|\sin\alpha_j$, respectively. The number of such terms in the expansion of Eq. (6) given by $j_{\max}$ will depend on the strength of the corrugation of the crystal surface and its degree of asymmetry. A great simplification is achieved by treating the first term ($j=1$) in Eq. (6) as the leading term and the remaining j terms as a perturbation. Now, by inserting Eq. (6) into Eq. (3) and performing the corresponding integration over the unit cell, we obtain [see the Appendix, Eq. (A5)] the following analytical solutions for the $\mathcal{V}_{\mathbf{G}}$ Fourier coefficients [$\mathbf{G}=(2\pi/d)(n,0)$] :

$$\mathcal{V}_{n0}=\sum_{k=-\infty}^{+\infty} i^{n+k} I_k(\beta_{11}) I_{n-k}(\beta_{21}) + \chi \sum_{k=-\infty}^{+\infty} i^{n+k} I_k(\beta_{11}) \sum_{j=2}^{j_{\max}} |h_j| [i^{-j} e^{i\alpha_j} I_{n-k-j}(\beta_{21}) + i^{j} e^{-i\alpha_j} I_{n-k+j}(\beta_{21})] + O(|h|^2), \quad (7)$$

where the I_k functions are the modified Bessel functions of integer order[40] with their arguments $\beta_{11}=-2\chi \mathrm{Re}(h_1)$ and $\beta_{21}=2\chi \mathrm{Im}(h_1)$. The first sum in this equation accounts for the leading term in the corrugation and the second sum accounts for the pertubation coming from the higher-order terms.

B. Close-coupling equations

Elastic diffraction probabilities for the scattering of a gas atom of mass μ and wave vector $\mathbf{k}$ from a rigid corrugated periodic surface were calculated by solving the well-known set of CC equations[33,35]

$$\left[\frac{\hbar^2}{2\mu}\frac{d^2}{dz^2}+E_{\mathbf{G}z}-V_0(z)\right]\psi_{\mathbf{G}}(z)=\sum_{\mathbf{G}'\neq\mathbf{G}} V_{\mathbf{G}'-\mathbf{G}}(z)\psi_{\mathbf{G}'}(z), \quad (8)$$

where $\psi_{\mathbf{G}}(z)$ is the diffracted wave function in the $\mathbf{G}$ diffraction channel, $V_0(z)$ is the bare potential [Eq. (4)], and $V_{\mathbf{G}'-\mathbf{G}}(z)$ are the coupling terms for the diffraction process [Eq. (5)]. $E_{\mathbf{G}z}$ is the z component of the kinetic energy of each diffraction channel and is given by

$$E_{\mathbf{G}z}=E_i-\frac{\hbar^2}{2\mu}\left|\sqrt{\frac{2\mu E_i}{\hbar^2}}\sin\theta_i(\cos\phi_i,\sin\phi_i)+\mathbf{G}\right|^2, \quad (9)$$

where E_i is the total incident beam energy and θ_i and ϕ_i are polar and azimuthal angles, respectively. Each diffraction channel is represented by an effective potential of the form $[V_0(z)+(\hbar^2/2\mu)(\mathbf{K}_i+\mathbf{G})^2]$, where $(\hbar^2/2\mu)(\mathbf{K}_i+\mathbf{G})^2$ can be seen as the asymptotic energy of the $\mathbf{G}$ channel. As has been discussed elsewhere,[33] in contrast to other types of scattering processes (e.g., atom-diatom scattering), surface diffraction is characterized by *moving thresholds*, that is, the asymptotic energies of the diffraction channels are functions depending on the set (E_i,θ_i,ϕ_i) through the $\mathbf{k}_i$ vector. For the one-dimensional corrugation ϕ_i will be considered zero. Equation (8) is solved with the usual boundary conditions.[33] The amplitude $S_{\mathbf{G}0}$ or the transition probability from the specular channel ($\mathbf{G}=0$) to the $\mathbf{G}$ diffraction channel is related to the diffraction intensity by $I_{\mathbf{G}}=|S_{\mathbf{G}0}|^2$.

In general, for stepped surfaces, the scattering is not parity reversal invariant[41] with respect to the scattering direction. The effect of the direction of approach of the atomic beam towards the surface, downhill or uphill scattering, should dramatically change the diffraction patterns only if the corrugation is asymmetric. For stepped surfaces it is observed that in downhill scattering positive momentum transfer values predominate, while for uphill scattering the negative values predominate.[42]

C. Effective corrugation function

Equipotential surfaces or contour plots can be obtained from the classical turning points of the potential Eq. (2), which are defined by the locus of all points such that[3] $V(\mathbf{R},z)=E_i$. The implicit function $z=\xi_{E_i}(\mathbf{R})$ is called the effective corrugation function and depends on the total energy E_i of the collision[43]

$$\xi_{E_i}(\mathbf{R})=\frac{1}{\chi}\ln\left[-\frac{D}{E_i}+\sqrt{\frac{D^2}{E_i^2}+\frac{D}{E_i}\left(1+\sum_{\mathbf{G}\neq 0}\frac{\mathcal{V}_{\mathbf{G}}}{\mathcal{V}_0}e^{i\mathbf{G}\cdot\mathbf{R}}\right)}\right]. \quad (10)$$

Unfortunately, this effective corrugation has the drawback that it does not increase monotonically with energy in the range of relevant energies (say, for example, 5–100 meV), but rather passes through a maximum and then decreases at higher collision energies, which is not expected from a good description of the effective corrugation.[3] This is one of the main drawbacks of the model potential Eq. (1). It can be overcome if the Fourier coefficients defined in Eq. (2) are modified at different incident energies of the atomic beam in order to obtain the correct behavior, that is, an increase in the corrugation with E_i.

For a one-dimensional corrugation, the sum over $\mathbf{G}$ under the square root in Eq. (10) can be expressed as

$$\sum_{\mathbf{G}\neq\mathbf{0}}\frac{\mathcal{V}_{\mathbf{G}}}{\mathcal{V}_0}e^{i\mathbf{G}\cdot\mathbf{R}}=\sum_{n=1}^{j_{\max}}\left|\frac{\mathcal{V}_{n0}}{\mathcal{V}_0}\right|\cos\left(\theta_{n0}+\frac{2\pi}{d}nx\right), \quad (11)$$

with $\tan\theta_{n0}=\mathrm{Im}(\mathcal{V}_{n0}/\mathcal{V}_0)/\mathrm{Re}(\mathcal{V}_{n0}/\mathcal{V}_0)$. Usually $D<E_i$ and therefore Eq. (10) can be linearized by expanding the square root and the natural logarithm in a Taylor-series expansion up to the first power of their arguments. With this linearization of the effective corrugation, analytical expressions of the diffraction intensities within the Eikonal approximation can be easily obtained as discussed in the next subsection.

D. Eikonal approximation for diffracted intensities

In the preceding subsection we have shown how it is possible to transform the model potential into an effective energy-dependent corrugation. In the next step we then use the Eikonal approximation to calculate the diffraction intensities to provide zeroth-order values of the corrugation parameters as inputs in the CC calculations at high energies. Following Garibaldi *et al.*,[44] the diffracted intensities can be expressed in the Eikonal approximation as

$$I_{\mathbf{G}}=\left|\frac{1}{S}\int_{\mathrm{U}} d\mathbf{R} e^{-i\mathbf{G}\cdot\mathbf{R}} e^{iq_{\mathbf{G}z}\xi(\mathbf{R})}\right|^2, \quad (12)$$

where $q_{\mathbf{G}z}$ is the z component of the momentum transfer $q_{\mathbf{G}}$ $(=\mathbf{k}_i-\mathbf{k}_f)$. Moreover, it is most accurate for small wavelengths of the incident atoms, relatively small corrugations, and small angles of incidence with respect to the normal. The main drawbacks of this approximation are that multiple scattering is not taken into account and that the calculated intensities are therefore independent of the azimuthal angle. Moreover, it is not possible to distinguish between $\xi(\mathbf{R})$ or $-\xi(\mathbf{R})$ as the profile for the electronic density. Also, the attractive potential is only approximately accounted for by the Beeby correction[45] in calculating $q_{\mathbf{G}_z}$. To account for the

softness of the repulsive potential, $\xi(\mathbf{R})$ is replaced by $\xi_{E_i}(\mathbf{R})$ from Eq. (10), which has been found to be a good starting point for a fitting procedure of the Fourier coefficients of the corrugation function. For one-dimensional corrugations, if the linearization of $\xi_{E_i}(\mathbf{R})$ is substituted into Eq. (12) and the corresponding integral is performed, the diffracted intensities are given by [see the Appendix, Eq. (A6)]

$$I_{n0} \approx \left| \sum_{k=-\infty}^{+\infty} i^k J_k(z_{11}) J_{n-k}(z_{21}) + \frac{i q_{nz}}{2} \sum_{k=-\infty}^{+\infty} i^k J_k(z_{11}) \sum_{j=2}^{j_{\max}} \left| \frac{\mathcal{V}_{j0}}{\mathcal{V}_0} \right| [e^{i\theta_{j0}} J_{n-k-j}(z_{21}) + e^{-i\theta_{j0}} J_{n-k+j}(z_{21})] \right|^2, \tag{13}$$

where, again, it has been assumed that the first coefficient $|\mathcal{V}_{10}/\mathcal{V}_0|$ (the leading term) gives the most important contribution to I_{n0} and the rest is taken as a perturbation. The J_k functions are the Bessel functions of integer order[40] and their arguments are defined by $z_{11} = q_{nz}\mathrm{Re}(\mathcal{V}_{10}/\mathcal{V}_0)$ and $z_{21} = q_{nz}\mathrm{Im}(\mathcal{V}_{10}/\mathcal{V}_0)$.

E. Corrections

In order to compare the theoretical diffraction intensities with the experimental ones several corrections must be accounted for. First of all, the calculations were performed for a perfect surface, while the real sample has defects. As pointed out in Sec. II, these defects result in a broadening and intensity decrease of some diffraction peaks. In order to compensate for this effect the integrated peak intensity was used instead of the peak maximum.[46]

Next we note that since the width of the diffraction peaks is comparable with the angular resolution (see Sec. III) small geometrical misalignments lead to a noticeable reduction of the peak intensity, which show up in the experiments when the intensity of individual peaks is optimized. From the average variation of the integrated intensity with the expected largest misalignments we estimate an error of $\pm 15\%$.

In the present experiment the angle between the incident and final beams is kept fixed and different parallel momentum transfers are scanned by rotating the target. This has the disadvantage that the intensities of all in-plane diffraction peaks for a given incident angle are not measured and the in-plane unitarity is not readily accessible. In this case, only one diffraction peak intensity can be obtained for a given incident angle by solving the CC equations. The relative diffraction intensities for different angles of incidence can be calculated for our geometry. Because of the unitarity of the CC peak intensities, there is a definite relationship between the intensities of a given diffraction peak calculated for different angles of incidence. This can be calculated and thus allows a comparison with the measured angular distribution for each incident energy.

Another correction is needed to account for the effective target area seen by the detector. Because of the fixed angle geometry the measured intensities depend on the visible and illuminated area of the sample, which is given by $A_i/\cos\theta_i$ where A_i is the area of the incident beam (its cross-sectional area) and the angle of incidence θ_i is measured with respect to the surface normal.[47] Analogously, the area of the surface that is seen by the detector is also given by $A_f/\cos\theta_f$, where A_f has the same meaning as A_i but for the diffracted beam and the *final* angle θ_f is also measured with respect to the same surface normal. Depending on the ratio of the areas, the effective area seen by the detector can be less or greater than the illuminated area. Thus a geometrical factor Λ has to be introduced. Its explicit expression is[47]

$$\Lambda = \frac{\min(A_i/\cos\theta_i, A_f/\cos\theta_f)}{A_i/\cos\theta_i}. \tag{14}$$

Finally, as the experiment is carried out at a finite crystal surface temperature T_S and the calculation corresponds to $T_S = 0$ K, the calculated diffracted intensities must be corrected using the Debye-Waller factor $2W$,

$$2W = \frac{3\hbar^2 T_S (k_{iz} + k_{fz})^2}{M k_B \Theta_D^2}, \tag{15}$$

with Θ_D the Debye temperature, M the mass of a surface atom, and k_B the Boltzmann constant. The acceleration from the attractive well depth D near the surface can be taken into account through the Beeby correction in which the z components of the initial and final wave vectors are replaced by

$$k_{i\mathrm{or}f,z} \rightarrow \sqrt{k_{i\mathrm{or}f,z}^2 + \frac{2\mu D}{\hbar^2}}. \tag{16}$$

For comparison with the experimental diffraction intensities, $I_{\mathbf{G}}^{\mathrm{expt}}$ is then calculated using the expression

$$I_{\mathbf{G}}^{\mathrm{expt}} = \Lambda e^{-2W} |S_{\mathbf{G}0}|^2, \tag{17}$$

where $|S_{\mathbf{G}0}|^2$ is the theoretical diffraction intensity at $T_S = 0$ K.

F. Fitting procedure

In a previous analysis[4] of the usual in-plane experimental configuration, in which all the in-plane diffraction peak intensities for a given incident energy and angle are collected, each diffraction pattern was fitted at each value of $E_{iz} = E_i \cos^2\theta_i$, resulting in as many sets of fitting corrugation parameters as pairs of values (E_i, θ_i). On the contrary, our effective corrugation functions only depend on E_i [see Eq. (10)], leading to a reduction in the number of fitting parameters for each diffraction pattern. As mentioned before, our fitting procedure for the corrugation parameters is based on analytical formulas for the potential Fourier coefficients and does not require any assumption about electron density profiles.[28] The only assumption made here has been to consider that a leading parameter is mainly responsible for the observed diffraction patterns, the rest being treated as a pertubation. Due to the asymmetry of the corrugation profiles the potential Fourier coefficients are complex and thus twice as many corrugation parameters (real and imaginary parts) have to be fitted. In addition, the well depth D and stiffness parameter χ of the Morse potential need to be determined. In

TABLE I. Effect of different sets of Morse potential parameters D, well depth, and χ, stiffness on the CC calculated intensities. These intensities correspond to the specular channel (00) and the first- (10) and second-order (20) diffraction channels for the system Cu(511) with $k_i = 6.14$ Å^{-1}.

D (meV)	χ(Å^{-1})	I_{00}^{CC}	I_{10}^{CC}	I_{20}^{CC}
5.35	1.05	0.2215	0.1513	0.3581
	1.50	0.2168	0.2727	0.2713
	2.00	0.0565	0.3382	0.0623
6.35	1.05	0.2652	0.0209	0.3975
	1.50	0.1301	0.3840	0.3093
	2.00	0.0242	0.3625	0.1394
7.35	1.05	0.0185	0.0012	0.2625
	1.50	0.1363	0.1399	0.2397
	2.00	0.0339	0.3955	0.1987

previous studies[3] for vicinal copper surfaces only the ratios of two potential Fourier coefficients $\mathcal{V}_{10}/\mathcal{V}_0$ and $\mathcal{V}_{20}/\mathcal{V}_0$ were considered for two incident energies (usually $\mathcal{V}_0$ is not calculated explicitly). Here, as our goal is to determine the corrugation for a wider range of collision energies, we have extended the Fourier series for the potential up to third order, which requires altogether six corrugation parameters. To avoid additional parameters, the values of D and χ of the Morse potential were fixed at 6.35 meV and 1.05 Å^{-1}, respectively, as determined experimentally for a CMP for vicinal Cu surfaces.[3] In connection with the D and χ values, it has been previously argued[3,4] that the diffraction intensities are much more affected by the stiffness parameter (χ) than by the well depth of the potential. Obviously, in any fitting procedure, it is sometimes difficult to know quantitatively the role played by one of the parameters because only the global effect of all potential parameters actually enters. To investigate the sensitivity of our CC calculations to the potential parameters we list in Table I the (00), (10), and (20) diffraction intensities for the Cu(511) surface at $k_i = 6.14$ Å^{-1} for various values of these two Morse parameters using the Fourier coefficients in Table II. As can be seen, with the variations shown in this table, the changes in the intensities are quite significant compared to the fitted intensities corresponding to $D = 6.35$ meV and $\chi = 1.05$ Å^{-1}. Thus, in fact, even though our fit is a good one we cannot claim that it is a unique one. Obviously, because of the large number of fit parameters even with the extensive experimental data base available here a unique fit involving all parameters is not feasible.

Thus the fitting procedure has been the following. First, to fit the experimental results for an incident energy of around 21 meV for the Cu(511) system we have taken the potential Fourier coefficients reported by Gorse *et al.*[3] as zeroth-order values. From our analytical formulas Eq. (7), we then deduce the corresponding corrugation parameters. These have been modified accordingly to fit our experimental diffraction intensities using CC calculations. At higher energies the initial departure has been to use the Eikonal formula Eq. (13) to obtain the zeroth-order values from the data. Next, we have assumed a linear variation[48] with the incident energy for all the corrugation parameters (real and imaginary parts) and take these values as zeroth-order values in subsequent CC calculations at intermediate collision energies. Again, at each incident energy, a series of CC calculations, in which mainly the three lowest-order corrugation coefficients were varied, were carried out to obtain better agreement with the experimental diffraction patterns. Thus we have covered the whole range of incident energies used in the experiment. For the Cu(211) system we have taken as trial values the ones corresponding to the Cu(511) system for two similar incident energies. In all our CC calculations a maximum of 17 diffraction channels have been used. Tests showed that with this basis set the S-matrix elements are calculated with three significant figures and the CC intensities are accurate to within $\pm 0.2\%$.

The quality of the fits can be seen in Fig. 4, where a comparison between the CC and experimental results at zero

TABLE II. Best fit ratios of the corrugation Fourier coefficients for the corrugated Morse potential at four different incident wave vectors of He atoms. The numbers in parentheses are the real and imaginary parts of the complex ratios in that order and the square brackets indicate powers of 10. Values of σ, defined in Eq. (18), are given in the last column.

System	k_i (Å^{-1})	$\mathcal{V}_0$	$\mathcal{V}_{10}/\mathcal{V}_0$	$\mathcal{V}_{20}/\mathcal{V}_0$	$\mathcal{V}_{30}/\mathcal{V}_0$	σ
Cu(511)	4.60	1.028	(0.163,2.29[-2])	(1.93[-2],5.37[-3])	(1.79[-3], 8.44[-4])	0.0167
	6.14	1.030	(0.170,2.33[-2])	(2.09[-2],5.65[-3])	(2.09[-3], 9.44[-4])	0.0108
	8.76	1.041	(0.197,2.41[-2])	(2.72[-2],6.60[-3])	(3.17[-3], 1.27[-3])	0.0064
	12.51	1.058	(0.233,2.57[-2])	(3.75[-2],8.17[-3])	(5.26[-3], 1.88[-3])	0.0092
Cu(211)	3.98	1.027	(0.160,2.14[-2])	(1.96[-2],4.37[-3])	(1.96[-3], 6.58[-4])	0.0493
	5.00	1.029	(0.169,2.13[-2])	(2.05[-2],4.48[-3])	(2.11[-3], 6.90[-4])	0.0262
	8.90	1.033	(0.180,2.15[-2])	(2.59[-2],5.10[-3])	(3.00[-3], 8.73[-4])	0.0077
	12.10	1.053	(0.222,2.16[-2])	(3.27[-2],5.87[-3])	(4.10[-3], 1.10[-3])	0.0095

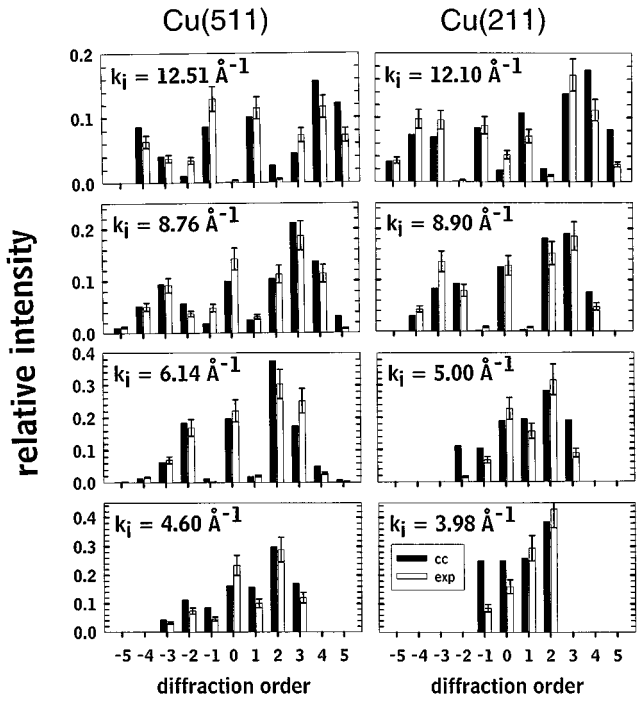

FIG. 4. Comparison of the experimental (white) and calculated close-coupling (black) diffraction intensities for different incident wave vectors. The experimental values shown here are determined by a one-dimensional integration over the diffraction peaks and have been corrected for the Debye-Waller factor. The CC intensities have been corrected by the geometrical factor Λ, defined in Eq. (14).

surface temperature is displayed at four incident wave vectors. In this figure we have plotted the diffraction order versus the relative intensity. The incident wave vectors chosen cover the entire range of the experiments. In the fit, our main concern has been to try to reproduce the whole diffraction pattern better than any particular diffraction intensity. The diffraction patterns are quite closely reproduced. As a measure of the goodness of the fits we have introduced the quantity σ defined by

$$\sigma = \frac{1}{N}\sqrt{\sum_{n=1}^{N} |I_n^{\mathrm{CC}} - I_n^{\mathrm{expt}}|^2}, \tag{18}$$

for each diffraction pattern, where N is the total number of experimentally observed diffraction channels. Clearly, the quality of a fit increases for smaller values of σ. σ is a function of the incident energy of the atoms and is listed in the last column of Table II.

V. DISCUSSION

In Table II, we present both for systems and for four different incident wave vectors of He atoms the corrugation Fourier coefficients obtained in our fitting procedure. As can be seen, for both surfaces the real coefficient $\mathcal{V}_0$ increases very smoothly with k_i. The remaining three columns give the relative magnitude of the higher Fourier coefficients appearing in Eq. (5). These values are complex and the real and imaginary parts are presented in parenthesis in that order. From an inspection of Table II, we observe that the strength of the couplings that can be determined from the modulus of the corresponding complex numbers also increases with k_i. For the Cu(211) case, the couplings are always slightly smaller than for the Cu(511) case. It should also be noted that the third potential Fourier coefficient becomes important with increasing collision energies, leading, together with the second Fourier coefficient, to a slight increase in the asymmetry of the effective corrugation profiles.

To examine the validity of the Eikonal approximation for scattering from stepped surfaces we compare the CC diffraction intensities with Eikonal results in Table III. For both systems, and for the smaller and higher k_i used in each case, two types of Eikonal results have been used. One is based on analytical results using the Eikonal approximation in its original formulation (Eik1) and the other includes the Beeby correction as well as the effective corrugation function Eq. (10) (Eik2). The large differences of both Eikonal approxi-

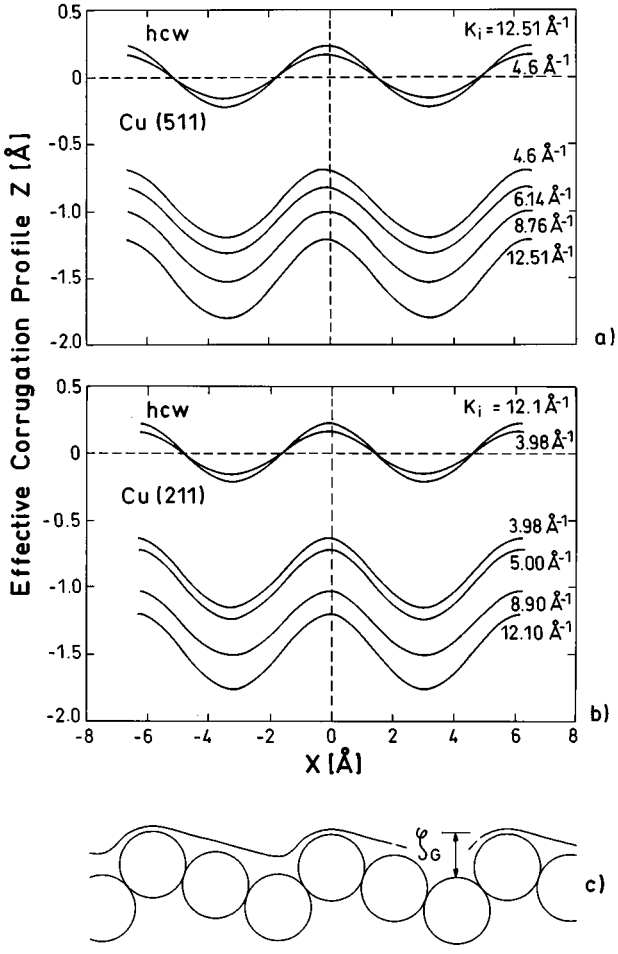

FIG. 5. Calculated effective corrugation functions for different incident beam energies (a) for the Cu(511) and (b) for the Cu(211) surface. Compared to the hard corrugated wall (HCW) the corrugated Morse potential has a higher corrugation and the loci of turning points come closer at the surface with increasing energy. (c) shows a schematic side view of the Cu(211) surface. ζ_G denotes the geometrical corrugation of the vicinal surface.

TABLE III. Comparison of theoretical diffraction intensities obtained from two Eikonal approximations [in its original form (Eik1) or when the Beeby correction and the effective corrugation function are taken into account (Eik2)] and from CC calculations for two k_i (the lowest and higher ones used in the experiments) without any corrections. The pair of integer numbers ($n0$) stand for the diffraction channel [$\mathbf{G}=(2\pi/d)(n,0)$]. *Numbers in square brackets indicate powers of* 10.

System	$n0$	I^{eik1}	I^{eik2}	I^{CC}	I^{eik1}	I^{eik2}	I^{CC}
Cu(511)		$k_i=4.60$ Å^{-1}			$k_i=12.51$ Å^{-1}		
	-50				1.53[-2]	8.72[-2]	
	-40				7.25[-2]	0.142	0.182
	-30	2.72[-4]	7.06[-3]	0.172	0.181	0.125	7.58[-2]
	-20	1.17[-2]	5.72[-2]	0.286	0.137	1.25[-2]	1.80[-2]
	-10	0.197	0.353	0.157	6.88[-3]	0.223	0.129
	00	0.578	0.228	0.220	0.176	3.77[-2]	7.05[-4]
	10	0.193	0.317	0.158	7.90[-3]	0.211	0.122
	20	1.19[-2]	5.75[-2]	0.288	0.128	2.80[-3]	2.86[-2]
	30	3.86[-4]	1.05[-2]	0.171	0.176	6.78[-2]	4.49[-2]
	40				7.94[-2]	0.137	0.157
	50				1.86[-2]	0.110	0.122
Cu(211)		$k_i=3.98$ Å^{-1}			$k_i=12.10$ Å^{-1}		
	-50				2.21[-2]	5.88[-2]	8.12[-2]
	-40				7.07[-2]	0.126	0.163
	-30				0.158	0.164	0.136
	-20	8.19[-3]	3.04[-2]	0.392	0.177	3.10[-2]	1.92[-3]
	-10	0.171	0.289	0.250	1.79[-2]	0.141	0.128
	00	0.645	0.399	0.251	0.259	0.108	2.52[-2]
	10	0.162	0.263	0.259	1.11[-2]	0.135	0.128
	20	9.01[-3]	3.25[-2]	0.396	0.150	1.74[-2]	2.19[-3]
	30	6.13[-4]	5.33[-3]	0.140	0.154	0.120	0.137
	40				9.07[-2]	0.141	0.174
	50				2.73[-2]	7.37[-2]	8.14[-2]

mations to the CC results reflect the effect of multiple scattering and the softness of the more realistic soft potentials fully accounted for in the CC calculation. Only at the highest energy do the Eik2 results come close to the CC intensities and then only for peaks with large intensities. But even then, in some cases, errors of nearly a factor 2 can occur.

The peak-to-peak amplitudes of the corrugation in the range of k_i values covered by the experiment are listed in Table IV. They extend from 0.51 Å to 0.58 Å for the Cu(511) surface and from 0.50 Å to 0.56 Å for the Cu(211) surface. In Ref. 3 only two peak-to-peak amplitudes were reported for the first surface: 0.52 Å at $k_i=6.3$ Å^{-1} and 0.56 Å at $k_i=11$ Å^{-1}, which are clearly in the range of the amplitudes obtained in this work. Our amplitude values come a bit closer to the predicted values of about 0.4 Å reported in Ref. 48. The corrugation amplitudes for a hard-sphere model of the surfaces also listed in Table IV are about a factor of 2.5 larger than measured.

VI. CONCLUSIONS

Diffraction intensities of He atoms scattered from vicinal Cu(211) and Cu(511) surfaces were measured and CC scattering calculations with a corrugated Morse potential were performed to fit a corrugation function with three complex Fourier coefficients. From a comparison with Eikonal calculations we conclude that hard corrugated wall Eikonal models are not adequate for the structural analysis of stepped surfaces as has sometimes been claimed in the literature.[4] The present CC calculations reveal that details of the interaction potential influence dramatically the effective corrugation leading to different shapes and peak-to-peak amplitudes of the effective corrugation function. In particular, our results show similar values for the $\mathcal{V}_{10}/\mathcal{V}_0$ ratio, but larger values for

TABLE IV. Peak-to-peak corrugation amplitudes in angstroms for the corrugated Morse potential ζ_{CMP} and for a hard corrugated wall potential ζ_{HCW} derived from the fitting procedure. For comparison, the geometrical corrugation ζ_G of a simple hard-sphere model of the surface is also listed.

System	ζ_G	k_i (Å^{-1})	ζ_{CMP}	ζ_{HCW}
Cu(211)	1.47	3.98	0.50	0.33
		12.10	0.56	0.44
Cu(511)	1.39	4.60	0.51	0.33
		12.51	0.58	0.46

the $\mathcal{V}_{20}/\mathcal{V}_0$ ratio than those reported in Ref. 3 also based on a soft wall repulsive potential, at similar incident wave vectors. Therefore, our effective corrugation profiles are somewhat more asymmetric, but overall the asymmetry is still small. At this point, we would like to stress that the Fourier coefficients of the corrugation and not of the potential should be taken as independent adjustable parameters, as can be seen in Eq. (7). The effective corrugation function is given in terms of these coefficients through Eq. (10). In Figs. 5(a) and 5(b) we have displayed the best fit effective corrugation profiles $\xi_{E_i}(x)$ for both systems. For comparison, in Fig. 5(c) we show also a schematic side view of the geometrical profile of the Cu(211) surface. With increasing k_i from 4.0 to 12.5 Å^{-1}, corresponding to an order of magnitude increase in the beam energy, we find only a slight increase of the asymmetry in the corrugation profile. From this we conclude that in order to probe the geometrical profile of the step atoms much higher beam energies (>300 meV) are required. Such a study would, however, have serious disadvantages. For one the more closely spaced peaks would be much more difficult to resolve and the much larger Debye-Waller factor would reduce the intensity and at the same time the multiphonon background would be greatly increased.

The present analysis of the electron density contours at large distances from the surface indicates that at the energies covered by the experiment their shapes are mainly determined by charge redistribution due to the Smoluchowski effect[21] rather than the geometrical positions of the atoms. Although scanning tunneling microscopy (STM) probes that surface at similar electron densities[49] as HAS, the lateral resolution of the STM at an atomic step is limited by the tip size, which hampers a high-resolution charge contour measurement.[50]

Finally, we note that very similar results for both the Cu(211) and Cu(511) surfaces were obtained, although they are known to have different electronic surface states. For the Cu(211) surface a terrace surface state similar to that of the Cu(111) surface has been found,[51] whereas for stepped surfaces with (100) terraces surface as the Cu(511) surface, a step localized state is observed.[52] Moreover, it has been shown that hybridization effects, which can lead to anticorrugation effects on smooth surfaces, are quite small compared to the corrugation since this is largely determined by the step geometry.[48]

ACKNOWLEDGMENTS

This research was supported by EEC Human Capital and Mobility Grant Contract No. ERBCHRXC930110 for S.M.-A. S.M.-A. thanks the MPI für Strömungsforschung for providing a stimulating environment during the realization of this work.

APPENDIX

In this appendix our goal is to solve analytically integrals of the form

$$T_n=\frac{1}{a}\int_{-a/2}^{a/2}dx e^{-i(2\pi/a)nx} \times \exp\left[i\alpha\sum_{j=1}^{j_{\max}} |\gamma_j|\cos\left(\eta_j+\frac{2\pi}{a}jx\right)\right], \quad \text{(A1)}$$

which are found in Sec. IV A [Eq. (3) for $\alpha=-i2\chi$] and in Sec. IV D [Eq. (12) for $\alpha=q_{\mathbf{G}z}$] and where now a stands for the unit cell length. The exponentials appearing in this integral can be expanded in Bessel functions of integer order J_n as[40]

$$e^{i\widetilde{\beta}_{1j}\cos(2\pi/a)jx}=\sum_{k=-\infty}^{+\infty} i^k J_k(\widetilde{\beta}_{1j})e^{ikj(2\pi/a)x},$$

$$e^{i\widetilde{\beta}_{2j}\sin(2\pi/a)jx}=\sum_{l=-\infty}^{+\infty} J_l(\widetilde{\beta}_{2j})e^{ilj(2\pi/a)x}, \quad \text{(A2)}$$

with $\widetilde{\beta}_{1j}=\alpha\gamma_j^r=\alpha|\gamma_j|\cos\eta_j$ and $\widetilde{\beta}_{2j}=-\alpha\gamma_j^i=-\alpha|\gamma_j|\sin\eta_j$. With Eq. (A2), the integral in Eq. (A1) is reduced to a product of simple exponential functions of the type $\exp[(2\pi/a)mx]$, where m is an integer number. In general, the parameters γ_j are small for higher j values and, frequently, we can take the exact contribution of the leading term (usually, $j=1$) and consider the rest of the terms as a perturbation. Doing this, Eq. (A1) can be rewritten as

$$T_n\approx\frac{1}{a}\int_{-a/2}^{a/2}dx e^{-i(2\pi/a)nx}e^{i\alpha|\gamma_1|\cos[\eta_1+(2\pi/a)x]} \times\left[1+i\alpha\sum_{j=2}^{j_{\max}}|\gamma_j|\cos\left(\eta_j+\frac{2\pi}{a}jx\right)\right]. \quad \text{(A3)}$$

Again, making use of Eq. (A2), Eq. (A3) is solved, yielding the result

$$T_n\approx\sum_{k=-\infty}^{+\infty} i^k J_k(\widetilde{\beta}_{11})J_{n-k}(\widetilde{\beta}_{21}) + \frac{i\alpha}{2}\sum_{k,l=-\infty}^{+\infty} i^k J_k(\widetilde{\beta}_{11})J_l(\widetilde{\beta}_{21}) \times\sum_{j=2}^{j_{\max}}|\gamma_j|[e^{i\eta_j}\delta_{k+l,n-j}+e^{-i\eta_j}\delta_{k+l,n+j}]. \quad \text{(A4)}$$

Now, if $\alpha=-i2\chi$ then $\widetilde{\beta}_{11}=i\beta_{11}$ and $\widetilde{\beta}_{21}=i\beta_{21}$, with $\beta_{11}=-2\chi\mathrm{Re}(h_1)$ and $\beta_{21}=2\chi\mathrm{Im}(h_1)$ [see Eq. (7)] and from Ref. 40, $J_k(\widetilde{\beta}_{11})=i^kI_k(\beta_{11})$ and $J_{n-k}(\widetilde{\beta}_{21})=i^{n-k}I_{n-k}(\beta_{21})$, with I_k being the modified Bessel function. Thus Eq. (A4) can be recast as

$$T_n \approx \sum_{k=-\infty}^{+\infty} i^{n+k} I_k(\beta_{11}) I_{n-k}(\beta_{21}) + \chi \sum_{k=-\infty}^{+\infty} i^{n+k} I_k(\beta_{11}) \times \sum_{j=2}^{j_{\max}} |\gamma_j| [i^{-j} e^{i\eta_j} I_{n-k-j}(\beta_{21}) + i^j e^{-i\eta_j} I_{n-k+j}(\beta_{21})]. \quad \text{(A5)}$$

$$T_n \approx \sum_{k=-\infty}^{+\infty} i^k J_k(z_{11}) J_{n-k}(z_{21}) + \frac{i q_{nz}}{2} \sum_{k=-\infty}^{+\infty} i^k J_k(z_{11}) \times \sum_{j=2}^{j_{\max}} |\gamma_j| [e^{i\eta_j} J_{n-k-j}(z_{21}) + e^{-i\eta_j} J_{n-k+j}(z_{21})], \quad \text{(A6)}$$

Finally, if $\alpha = q_{\mathbf{G}z}$ with $\mathbf{G} = (2\pi/a)(n,0)$, then Eq. (A4) gives the result of the Eikonal approximation with $j=1$ as the leading term:

with $z_{11} = q_{nz}\gamma_1^r = q_{nz}\mathrm{Re}(\mathcal{V}_{10}/\mathcal{V}_0)$ and $z_{21} = q_{nz}\gamma_1^i = q_{nz}\mathrm{Im}(\mathcal{V}_{10}/\mathcal{V}_0)$ [see Eq. (13)].

*Permanent address: Instituto de Matematicas y Fisica Fundamental, C/Serrano 123, 28006 Madrid, Spain.

[1] *Kinetics of Ordering and Growth at Surfaces*, edited by M.G. Lagally (Plenum, New York, 1990).

[2] J. Lapujoulade, Y. Lejay, and N. Papan, Surf. Sci. **90**, 133 (1979).

[3] D. Gorse, B. Salanon, F. Fabre, A. Kara, J. Perreau, G. Armand, and J. Lapujoulade, Surf. Sci. **147**, 611 (1984).

[4] D.S. Kaufman, R.M. Aten, E.H. Conrad, L.R. Allen, and T. Engel, J. Chem. Phys. **86**, 3682 (1987).

[5] J. Wollschläger, E.Z. Luo, and M. Henzler, Surf. Sci. **257**, 274 (1991).

[6] F. Fabre, D. Gorse, B. Salanon, and J. Lapujoulade, J. Phys. (Paris) **48**, 1017 (1987).

[7] E.H. Conrad, R.M. Aten, D.S. Kaufmann, L.A. Allen, T. Engel, M. den Nijs, and E.K. Riedel, J. Chem. Phys. **84**, 1015 (1986); **85**, 4856E (1986).

[8] H.H. Ernst, R. Folkerts, and L. Schwenger, Phys. Rev. B **52**, 8461 (1995).

[9] B.J. Hinch, A. Lock, H.H. Madden, J.P. Toennies, and G. Witte, Phys. Rev. B **42**, 1547 (1990).

[10] M. Sotto, Surf. Sci. **260**, 235 (1992).

[11] H.J. Ernst, F. Fabre, R. Folkerts, and J. Lapuloulade, Phys. Rev. Lett. **72**, 112 (1994).

[12] B.J. Hinch, A. Lock, J.P. Toennies, and G. Zhang, Europhys. Lett. **10**, 341 (1989).

[13] A. Lock, B.J. Hinch, and J.P. Toennies, in *Kinetics of Ordering and Growth at Surfaces* (Ref. 1), p. 77.

[14] A.M. Rodriguez, G. Bozzolo, and J. Ferrante, Surf. Sci. **289**, 100 (1993), and references therein.

[15] P. Jiang, F. Jona, and P.M. Marcus, Phys. Rev. B **35**, 7952 (1987).

[16] D.L. Adams and C.S. Sorensen, Surf. Sci. **166**, 495 (1986); D.L. Adams, V. Jensen, X.F. Sun, and J.H. Vollesen, Phys. Rev. B **38**, 7913 (1988).

[17] Q.F. Jiang, P. Statiris, T. Gustafsson, P. Haberle, and D.M. Zehner, J. Vac. Sci. **10**, 2197 (1992).

[18] H. Wagner, in *Solid Surface Physics*, Springer Tracts in Modern Physics Vol. 85 (Springer-Verlag, Berlin, 1979).

[19] R.L. Schwoebel and E.J. Shipsey, J. Appl. Phys. **37**, 3682 (1966); R.L. Schwoebel, *ibid.* **40**, 614 (1969).

[20] S.C. Wang and G. Ehrlich, Phys. Rev. Lett. **67**, 2509 (1991).

[21] R. Smoluchowski, Phys. Rev. B **24**, 754 (1931).

[22] J. Tersoff and L.M. Falicov, Phys. Rev. B **24**, 754 (1981).

[23] J.S. Nelson and P.J. Feibelmann, Phys. Rev. Lett. **68**, 2188 (1992).

[24] M.C. Desjouqueres and F. Cyrot-Lackmann, Solid State Commun. **18**, 1127 (1976).

[25] B.J. Hinch, Surf. Sci. **221**, 346 (1989).

[26] J. Lapujoulade and Y. Lejay, Surf. Sci. **69**, 354 (1977).

[27] J. Perreau and J. Lapujoulade, Surf. Sci. **122**, 342 (1982).

[28] N. Esbjerg and J.K. Nørskov, Phys. Rev. Lett. **45**, 807 (1980).

[29] P. Cortona, M.G. Dondi, and F. Tommasini, Surf. Sci. Lett. **261**, L35 (1992).

[30] L. Niu, D.J. Gaspar, and S.J. Sibener, Science **268**, 847 (1995).

[31] L. Niu, D.D. Koleske, D.J. Gaspar, and S.J. Sibener, J. Chem. Phys. **102**, 9077 (1995).

[32] G. Witte, J. Braun, A. Lock, and J.P. Toennies, Phys. Rev. B **52**, 2165 (1995).

[33] M. Hernandez, O. Roncero, S. Miret-Artes, P. Villarreal, and G. Gelgado-Barrio, J. Chem. Phys. **90**, 3823 (1989).

[34] E. Kirsten and K.H. Rieder, Surf. Sci. **265**, 67 (1992).

[35] M. Hernandez, S. Miret-Artes, P. Villarreal, and G. Delgado-Barrio, Surf. Sci. **274**, 21 (1992).

[36] G. Armand and J. R. Manson, Surf. Sci. **119**, L299 (1982).

[37] F. Hofmann, J.P. Toennies, and J.R. Manson, J. Chem. Phys. **101**, 10 155 (1994).

[38] Since a stepped surface can be described as a convolution of a finite terrace with a regular step lattice, the resulting LEED pattern can be thought of as a product of the diffraction pattern from the terraces and the step lattice (Ref. 39). Therefore Bragg conditions exist whenever the diffraction maxima for terrace and steps coincide, while at anti-Bragg conditions terrace diffraction minima coincide with step diffraction maxima. However, the intensity observed with LEED is mainly determined by the terrace diffraction. In contrast, for HAS virtually no diffraction results from the low index terraces since for helium atoms they are very smooth. However, the step atoms have an enlarged form factor for the He surface interaction potential that give rise to multiple scattering and thus a modulation of the diffraction intensity with perpendicular momentum transfer.

[39] M. Henzler, Appl. Phys. A **34**, 205 (1984).

[40] *Handbook of Mathematical Functions*, edited by M. Abramowitz and I. A. Stegun (Dover, New York, 1972).

[41] M. Hernandez, S. Miret-Artes, P. Villarreal, and G. Delgado-Barrio, Surf. Sci. **290**, L693 (1993).

[42] B.J. Hinch, A. Lock, J.P. Toennies, and G. Zhang, J. Vac. Sci. Technol. B **7**, 1260 (1989).

[43] Note that Eq. (10) corrects the error of the corresponding equation in Ref. 3.

[44] U. Garibaldi, A. C. Levi, R. Spadacini, and G. E. Tommei, Surf. Sci. **48**, 649 (1975).

[45] J. L. Beeby, J. Phys. C **4**, L359 (1977).

[46] Since the diffraction peaks show no significant broadening along the steps (see Fig. 3), the intensity was summed up only perpendicular to the steps as recorded in the angular distribution.

[47] J.P. Toennies, in *Surface Phonons*, edited by W. Kress and F.W. de Wette, Springer Series in Surface Sciences Vol. 21 (Springer-Verlag, Berlin, 1990).

[48] J. F. Annett, Phys. Rev. B **35**, 7826 (1987).

[49] J. Tersoff and D.R. Hamann, Phys. Rev. Lett. B **50**, 1998 (1983).

[50] G. Meyer, B. Neu, and K.H. Rieder, Chem. Phys. Lett. **240**, 379 (1995).

[51] R.F. Davis, R.S. Williams, S.D. Kevan, P.S. Wehner, and D.A. Shirley, Phys. Rev. B **31**, 1997 (1985).

[52] J.E. Ortega, F.J. Himpsel, P. Haight, and D.R. Peale, Phys. Rev. B **49**, 13 859 (1994).